Optimising the relaxivities of Mn^{2+} complexes by targeting human serum albumin (HSA)[i]

Attila Forgács[a], Lorenzo Tei[a], Zsolt Baranyai[b], David Esteban-Gómez[c], Carlos Platas-Iglesias[c*] and Mauro Botta[a†]

[a] Dipartimento di Scienze e Innovazione Tecnologica, Università del Piemonte Orientale "A. Avogadro", Viale T. Michel 11, 15121 Alessandria, Italy

[b] Department of Inorganic and Analytical Chemistry, University of Debrecen, Egyetem tér 1., H-4010, Debrecen, Hungary

[c] Universidade da Coruña, Centro de Investigacións Científicas Avanzadas (CICA) and Departamento de Química, Facultade de Ciencias, 15071, A Coruña, Galicia, Spain

How to cite:

Abstract

We report two novel macrocyclic ligands based on the 1,4-DO2AM platform (1,4-DO2AM = 2,2′-(1,4,7,10-tetraazacyclododecane-1,4-diyl)diacetamide) and containing two benzyl groups attached either to the nitrogen atoms of the macrocyclic unit (1,4-BzDO2AM) or to the amide pendant arms (1,4-DO2AMBz). The protonation constants of the ligands and the stability constants of their Mn^{2+} complexes were determined using pH potentiometry. The introduction of benzyl groups results in a slight decrease of the stability constants of the Mn^{2+} complexes and a slight increase of their acid-catalysed dissociation reactions. A detailed relaxometric characterisation of the complexes using nuclear magnetic dispersion relaxation (NMRD) and ^{17}O NMR studies indicated that the increase in molecular weight associated with the presence of benzyl groups results in a remarkable increase of proton relaxivities r_{1p}, which take values of 3.8, 3.5 and 2.5 mM^{-1} s^{-1} for [Mn(1,4-BzDO2AM)]$^{2+}$, [Mn(1,4-DO2AMBz)]$^{2+}$ and [Mn(1,4-DO2AM)]$^{2+}$ (at 25 °C and 20 MHz). The [Mn(1,4-BzDO2AM)]$^{2+}$ and [Mn(1,4-DO2AMBz)]$^{2+}$ complexes form relatively strong adducts with Human Serum Albumin (HSA) with association constants of $(3.9 \pm 0.6) \times 10^3$ and $(2.0 \pm 0.3) \times 10^3$ M^{-1}, respectively. The interaction with the protein slows down the rotational tumbling of the complex in solution, which results in adducts endowed with remarkably high proton relaxivities ($r_{1p}{}^{b} = 18.5 \pm 0.7$ and 27.4 ± 1.4 mM^{-1} s^{-1} for [Mn(1,4-BzDO2AM)]$^{2+}$ and [Mn(1,4-DO2AMBz)]$^{2+}$, respectively).

Keywords: MRI contrast agents; DFT calculations; manganese complexes; relaxivity; human serum albumin

* carlos.platas.iglesias@udc.es

† mauro.botta@uniupo.it

Introduction

Derivatives of the tetraaza macrocycle 1,4,7,10-tetraazacyclododecane (cyclen) functionalised with different types and numbers of pendant arms have been investigated in detail in the last few decades due to several successful applications of their metal complexes.[1] For example, lanthanide complexes of such ligands have proved useful as magnetic resonance imaging (MRI) contrast agents,[2] radiopharmaceuticals for nuclear medicine techniques,[3] Chemical Exchange Saturation Transfer (CEST) agents,[4] and luminescent probes.[5] The tetraacetic acid derivative (DOTA) is probably the most utilised, since it forms metal complexes characterised by high thermodynamic stability and marked kinetic inertness towards dissociation, hence favouring their use in *in vivo* applications.[6]

Complexes of Mn^{2+} containing coordinated water molecules have been attracting increasing attention due to their potential application as MRI contrast agents.[7,8] We have recently initiated a research program to develop Mn^{2+} complexes that could represent an alternative to the classical Gd^{3+} MRI contrast agents.[9–12] We have shown that Mn^{2+} complexes containing one or two water molecules coordinated to the metal ion present relaxation efficiencies comparable to those of the commercially available Gd^{3+} agents.[11] Furthermore, we and others developed a family of macrocyclic and non-macrocyclic ligands containing lipophilic units that form micelles in solution and rather stable adducts with HSA, which results in relatively high relaxivities due to the elongation of the tumbling time of the complex in solution.[13–15] Besides a potential lower toxicity of the Mn^{2+} complexes compared to the Gd^{3+} counterparts, redox responsive agents based on the Mn^{2+}/Mn^{3+} pair were also proposed.[16]
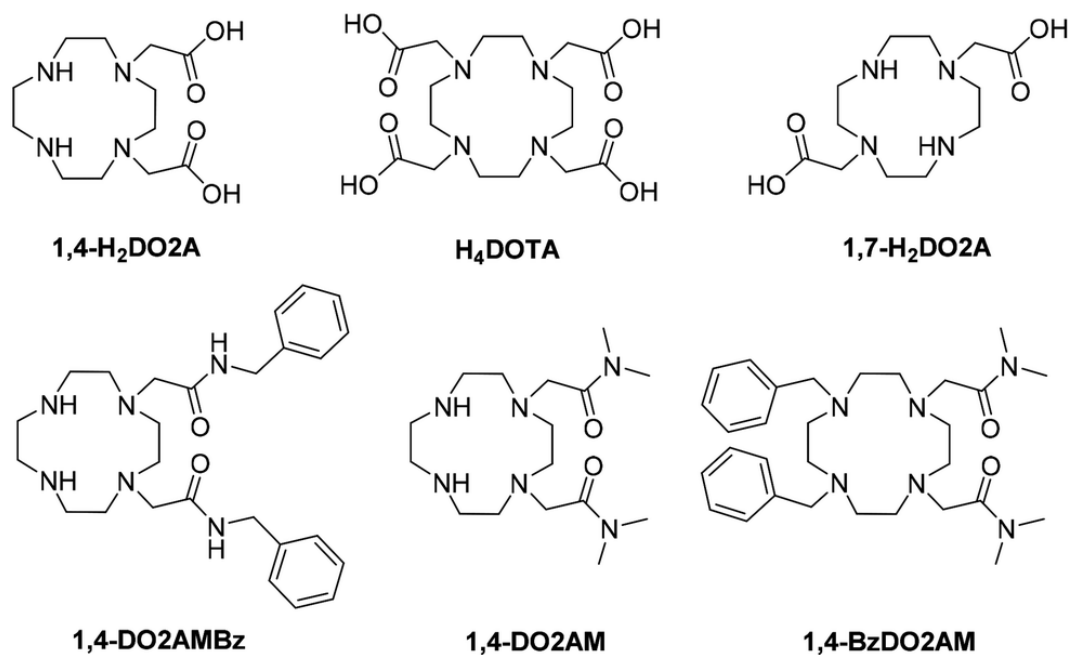

Scheme 1. Structures of the ligands discussed in this work.

Macrocyclic ligands often form metal complexes with higher thermodynamic stability and kinetic inertness than related non-macrocyclic analogues. In the context of MRI agents, the stable complexation of the target metal ion is of great importance to avoid the release of the toxic free metal ion *in vivo*. For instance, the stability constants of Mn^{2+} complexes of cyclen-based ligands containing acetate pendant arms were studied in aqueous solution by means of potentiometric and microcalorimetric techniques, which afforded log K, $\Delta H°$ and $T\Delta S°$ values for the complexation reactions. The metal complexes present high stability constants

due to both favourable enthalpic and entropic contributions. With the unique exception of DOTA (1,4,7,10-tetraazacyclododecane-1,4,7,10-tetraacetic acid, Scheme 1), the entropic term is prevalent. Furthermore, it was also noticed that 1,4-H_2DO2A (1,4,7,10-tetraazacyclododecane-1,4-diacetic acid) forms a more stable complex than the 1,7-H_2DO2A isomer.[17,18] The stability constant of the Mn^{2+} complex with the bis-amide derivative 1,4-DO2AM was found to be 2.5 log K units lower than that of [Mn(1,4-DO2A)]. However, the bis-amide ligand was found to be remarkably inert with respect to dissociation, with a dissociation half-life at pH 7.4 $ca.$ 10 times higher than that of [Mn(1,4-DO2A)].[19]

We envisaged expanding the family of macrocyclic Mn^{2+} complexes based on cyclen while introducing hydrophobic units to target HSA. Towards this aim, we present here the cyclen-based ligands 1,4-DO2AMBz and 1,4-BzDO2AM (Scheme 1), which contain two acetamide pendants at positions 1 and 4 of the cyclen ring and two benzyl groups either at positions 7 and 11 of the macrocycle (1,4-BzDO2AM) or as N-substitution of the acetamide pendants (1,4-DO2AMBz). The presence of two hydrophobic moieties favours the formation of adducts with Human Serum Albumin (HSA)[20] through non-covalent interactions. We report a detailed investigation of the thermodynamic stability and dissociation kinetics of the Mn^{2+} complexes, as well as a ^1H and ^{17}O NMR relaxometric study to determine the parameters that govern the relaxivity of these complexes. Finally, the interaction of the complexes with HSA was assessed using relaxometric techniques.
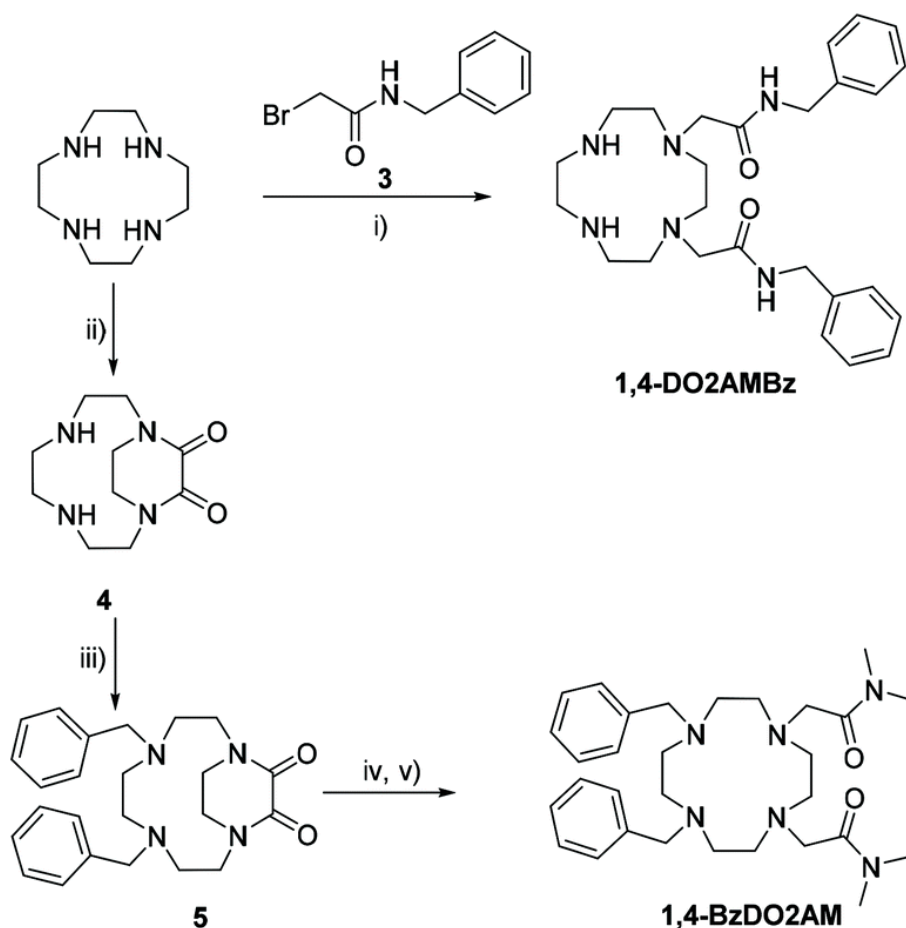
Scheme 2. Synthesis of the ligands. (i) CH_3CN, K_2CO_3, Δ, 24 h; (ii) diethyloxalate, EtOH, Δ, 24 h;
(iii) benzyl bromide, CH_3CN, K_2CO_3, Δ, 24 h; (iv) 5 M NaOH, Δ, 24 h;
(v) N,N-dimethyl 2-chloroacetamide, CH_3CN, K_2CO_3, Δ, 24 h.

Results and discussion

Synthesis of the ligands

The 1,4-DO2AMBz ligand was synthesised in two steps involving the preparation of sidearm **3** by a reaction of 2-bromoacetyl bromide and benzyl amine,[21] followed by the regioselective *cis* alkylation of cyclen,[22] which provided the 1,4-DO2AMBz ligand in *ca.* 20% yield over the two steps after semi-preparative HPLC purification. The 1,4-BzDO2AM ligand was synthesised starting from cyclen, which was converted into 1,4-dibenzyl-1,4,7,10-tetraazacyclotetradecane following the method of Handel.[23] Thus, cyclen was protected using diethyl oxalate to give intermediate **4** (Scheme 2), which was subsequently alkylated with benzyl bromide using K_2CO_3 as a base. Basic deprotection of compound **5** and alkylation of the resulting intermediate with *N,N*-dimethyl 2-chloroacetamide gave the 1,4-BzDO2AM ligand in a decent 20% yield over the four steps.

Ligand protonation constants and stability constants of the Mn^{2+} complexes

The protonation constants of 1,4-DO2AMBz and 1,4-BzDO2AM ligands, defined in eqn (1), were determined by pH-potentiometry in 0.1 M KCl aqueous solution. The log K_i^H values are compared with those of 1,4-DO2AM, 1,4-DO2A^{2-}, 1,7-DO2A^{2-} and DOTA^{4-} in Table 1.

$$K_i^H = \frac{[H_iL]}{[H_{i-1}L][L]} \quad \text{with } i = 1, 2, \dots, 6. \tag{1}$$

Table 1. Ligand protonation constants and stability and protonation constants of the corresponding Mn^{2+} complexes determined using potentiometric titrations (25 °C, 0.1 M KCl) [a]

	1,4-BzDO2AM	1,4-DO2AMBz	1,4-DO2AM [b]	1,4-DO2A^{2-} [c]	1,7-DO2A^{2-} [c]	DOTA^{4-} [d]
log K_1^H	11.11(1)	9.62(3)	10.14	11.40	11.66	11.41
log K_2^H	8.22(4)	6.90(5)	8.38	9.58	9.75	9.83
log K_3^H	—	—	—	3.74	4.06	4.38
log K_4^H	—	—	—	1.65	1.78	4.63
log K_5^H	—	—	—	—	—	1.92
log K_6^H	—	—	—	—	—	1.58
$\sum$log K_i^H	19.33	16.52	18.52	26.37	27.25	33.75
log K_{MnL}	11.54(4)	10.72(3)	12.64	15.22	15.07	19.33
log K_{MnLH}	—	—	—	4.15	4.09	—
log K_{MnLH_2}	—	—	—	—	3.70	—
log $K_{MnLH_{-1}}$	10.44(5)	9.44(7)	—	—	—	—
pMn [e]	6.00	6.69	6.94	7.03	6.75	9.02

[a] Standard deviations (3σ) are shown in parentheses. [b] Ref. 19. [c] Ref. 17. [d] Ref. 26. [e] Defined as −log[Mn]$_{free}$ with pH = 7.4, [Mn^{2+}] = [L] = 10^{-5} M.

The protonation scheme of 1,4-DO2AM has been studied in detail using both ^{1}H-NMR spectroscopy and pH-potentiometry methods.[19] Because of the similarities of 1,4-BzDO2AM, 1,4-DO2AMBz and 1,4-DO2AM, we can assume that the first protonation occurs on the nitrogen atoms of the macrocycles N1 and N4, which are functionalised with the acetamide pendant arms (the protonation involves partially both N-atoms). The second protonation takes place on the unsubstituted (1,4-DO2AMBz) or benzyl-substituted (1,4-BzDO2AM) nitrogen atom N7 (or N10) to afford a *trans* bis-protonated species on N1/N7 or N4/N10. The protonation of *trans* nitrogen atoms minimises the electrostatic repulsion by allowing a larger charge separation of the protonated sites.[24]

Comparison of the protonation constants of 1,4-BzDO2AM and 1,4-DO2AMBz with those of 1,4-DO2AM indicates that the log K_1^H value of 1,4-BzDO2AM is slightly higher, whereas the log K_1^H and log K_2^H values of 1,4-DO2AMBz are significantly lower than those of 1,4-DO2AM. The basicity of the ring N-donor atoms might be influenced by four factors: (i) the electron withdrawing effect of the amide groups that reduces the basicity of the nitrogen donor atoms; (ii) the electron donor or acceptor behaviour of the substituents on the amide group; (iii) the electrostatic repulsion between the protonated ring N-donor atoms resulting in a lower basicity of the ring amines and (iv) the formation of H-bonding interaction between the protonated nitrogen and the amide O-donor atoms that could increase the amine basicity.[25] Likely, the contribution of all these processes is responsible for the lower log K_i^H values of the nitrogen donor atoms of 1,4-DO2AMBz as compared to 1,4-DO2AM. The total basicity ($\sum$log K_i^H) of 1,4-BzDO2AM is comparable to that of 1,4-DO2AM, whereas the $\sum$log K_i^H value of 1,4-DO2AMBz is significantly lower (Table 1).

The stability constants of the Mn^{2+} complexes of 1,4-BzDO2AM and 1,4-DO2AMBz are defined in eqn (2):

$$K_{ML} = \frac{[ML]}{[M][L]} \tag{2}$$

The stability constants of the 1,4-BzDO2AM and 1,4-DO2AMBz complexes have been calculated from the titration curves obtained at 1 : 1 metal to ligand concentration ratios. The best fits of the experimental data (volume of KOH added *vs.* pH) were obtained by using the model that involves the formation of ML species at equilibrium. However, the titration data of the Mn^{2+}-1,4-BzDO2AM and Mn^{2+}-1,4-DO2AMBz systems indicated the consumption of base at pH > 8.5 due to the formation of hydroxide species. This process was characterised by the equilibrium constant $K_{MLH_{-1}}$ defined according to eqn (3):

$$K_{MLH_{-1}} = \frac{[ML]}{[MLH_{-1}][H^+]} \tag{3}$$

The stability constants of the Mn^{2+} complexes formed with 1,4-BzDO2AM and 1,4-DO2AMBz are about 1 and 2 orders of magnitude lower than that of [Mn(1,4-DO2AM)]$^{2+}$, respectively. The lower log K_{ML} value determined for the [Mn(1,4-DO2AMBz)]$^{2+}$ complex is not surprising, as the total basicity of 1,4-DO2AMBz is about 2 log K units lower than that of 1,4-DO2AM. However, the stability constant of the [Mn(1,4-BzDO2AM)]$^{2+}$ complex is significantly lower than expected by taking into account the $\sum$log K_i^H values presented in Table 1. Because of the similar basicity of the N donor atoms in 1,4-BzDO2AM and 1,4-DO2AM ligands, it can be assumed that the presence of the two bulky benzyl substituents introduces some

steric constraints for the coordination of the ligand to the relatively small Mn^{2+} ion (97 pm for coordination number six, high-spin configuration).[27]

It should be noted that MnL complexes formed with 1,4-BzDO2AM, 1,4-DO2AMBz and 1,4-DO2AM ligands are characterised by lower stability constants than Mn(1,4-DO2A), Mn(1,7-DO2A), Mn(DO3A) and Mn(DOTA) complexes. The lower log K_{ML} values of the Mn^{2+}-complexes formed with 1,4-DO2A-bisamide ligands can be explained by the lower affinity of Mn^{2+} ions to the non-charged amide oxygens with respect to the charged carboxylate O-donors and/or the significantly lower basicity ($\sum \log K_i^H$) of the ring N-atoms. The complexes of 1,4-BzDO2AM and 1,4-DO2AMBz form hydroxo species at pH values above *ca.* 8.0 and 7.0, respectively (Fig. 1). The complexes dissociate at relatively high pH, with 2.6% of the total Mn^{2+} being in the form of the aqua ion at pH 6.0 for the Mn^{2+}:1,4-BzDO2AM system and 22% for the Mn^{2+}:1,4-DO2AMBz system ([L] = [Mn^{2+}] = 10^3 M). Thus, the [Mn(1,4-DO2AMBz)]$^{2+}$ complex is somewhat more stable about neutral pH than the [Mn(1,4-BzDO2AM)]$^{2+}$ analogue. This is also reflected in the pMn values (Table 1), which provide an indication of the stability of the complex at pH 7.4.
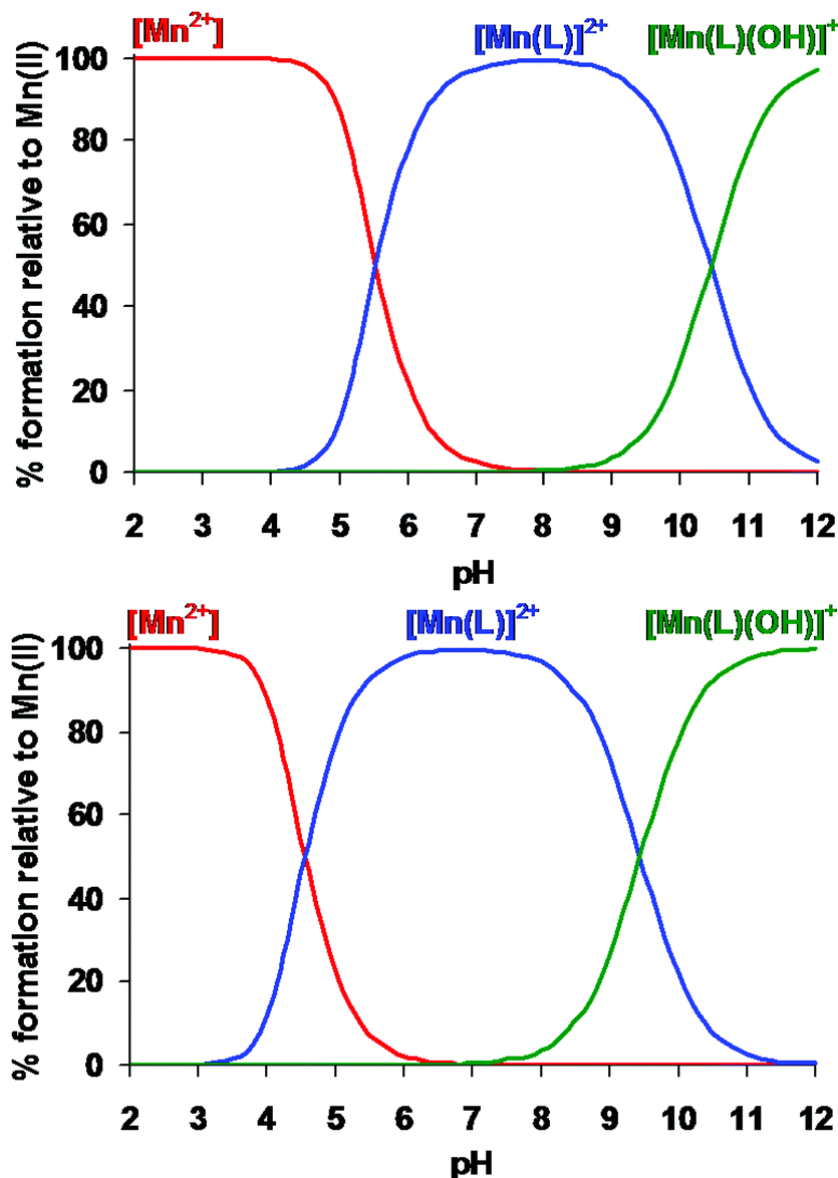

Fig. 1. Species distribution diagrams calculated for the 1,4-BzDO2AM:Mn^{2+} (top) and 1,4-DO2AMBz:Mn^{2+} (bottom) systems. [L] = [Mn^{2+}] = 10^{-3} M.

Transmetallation kinetics

Before *in vivo* application, it is important to evaluate the kinetic inertness of any metal-complex and thus the possible release of free metal ions or ligands in the body.[28] The kinetic inertness of a metal complex is characterised by the rates of its dissociation, which is typically measured under strongly acidic conditions ($[H^+] > 1.0$ M).[29] However, since these conditions differ considerably from the physiological ones, it is crucial to also consider the transmetallation reactions occurring with endogenous metal ions (Cu^{2+}, Zn^{2+} and Ca^{2+}) at physiological pH. In fact, a Mn^{2+} complex in body fluids may interact with these ions resulting in the release of the Mn^{2+}-ion. Therefore, in order to assess the kinetic inertness, the rates of the transmetallation reactions of Mn^{2+}complexes with Cu^{2+} and Zn^{2+} ions are typically determined in the pH range 2–7.[18,19,26] For Mn^{2+} DOTA-like complexes the metal ion is slowly released through the proton-assisted dissociation pathway, whereas the dissociation rate is generally not altered by the presence of Zn^{2+} and Cu^{2+}.[18,19,26] For the direct comparison of the kinetic properties of $[Mn(1,4\text{-BzDO2AM})]^{2+}$ and $[Mn(1,4\text{-DO2AMBz})]^{2+}$ with those of $[Mn(1,4\text{-DO2AM})]^{2+}$, $[Mn(1,4\text{-DO2A})]$, $[Mn(1,7\text{-DO2A})]$ and $[Mn(DOTA)]^{2-}$, the method and the conditions used were the same as those previously reported.[18,19,26] Thus, the rates of the transmetallation reactions of $[Mn(1,4\text{-BzDO2AM})]^{2+}$ and $[Mn(1,4\text{-DO2AMBz})]^{2+}$ were determined by relaxometry at 20 MHz and 25 °C in the pH range 4.5–6.5 using Zn^{2+} as the exchanging metal ion (eqn (4); L denotes either 1,4-BzDO2AM or 1,4-DO2AMBz).

$$MnL + Zn^{2+} \leftrightarrows ZnL + Mn^{2+} \tag{4}$$
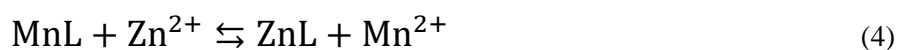
A 10- and 20-fold excess of Zn^{2+}-ions were used in order to apply a pseudo-first-order kinetic model. Then, the rates of the reaction can be expressed using eqn (5):

$$-\frac{d[MnL]_t}{dt} = k_d[MnL]_{tot} \tag{5}$$

where k_d is a pseudo-first-order rate constant and $[MnL]_t$ and $[MnL]_{tot}$ are the concentrations of the MnL species at time t and the total concentration of the complex, respectively. The calculated pseudo-first order rate constants for the transmetallation reaction of $[Mn(1,4\text{-BzDO2AM})]^{2+}$ and $[Mn(1,4\text{-DO2AMBz})]^{2+}$ with Zn^{2+} as a function of $[H^+]$ are shown in Fig. 2 (see also Fig. S7–S9, ESI[i]).

The rates of the transmetallation reactions are directly proportional to the H^+ concentration and independent of the concentration of Zn^{2+}. The increase in the k_d values with increasing $[H^+]$ can be interpreted in terms of the relatively slow proton assisted dissociation of the complex, followed by a fast reaction between the free ligand and the exchanging Zn^{2+} ions. The dependence of k_d on $[H^+]$ can be expressed as a first-order function of $[H^+]$ by taking into account the proton-independent (eqn (6)) and proton assisted pathways (eqn (7)), which are characterised by rate constants k_0 and k_1, respectively:

$$MnL \xrightarrow{k_0} Mn^{2+} + L \tag{6}$$

$$MnL + H^+ \xrightarrow{k_1} Mn^{2+} + HL \qquad (7)$$

By taking into account all possible pathways the pseudo-first-order rate constant (k_d) can be expressed by the following linear relationship:

$$k_d = k_0 + k_1[H^+] \qquad (8)$$

The fits of the experimental k_d values provided small values of k_0 with large standard deviations, which indicates that the spontaneous dissociation pathway does not contribute significantly to the dissociation of the complex under the applied conditions. The k_1 rate constants characterising the proton-assisted dissociation of the $[Mn(1,4\text{-}BzDO2AM)]^{2+}$ and $[Mn(1,4\text{-}DO2AMBz)]^{2+}$ complexes (Table 2) are about 4 times higher than that of $[Mn(1,4\text{-}DO2AM)]^{2+}$, but about three times smaller than those of the $[Mn(1,4\text{-}DO2A)]$ and $[Mn(1,7\text{-}DO2A)]$ complexes. It is generally accepted that the proton assisted dissociation of Mn^{2+} complexes of DOTA-like ligands containing carboxylate pendant arms takes place by protonation at one of the carboxylate groups, which is then likely followed by proton transfer to the ring nitrogen, resulting in the cascade-like de-coordination of each donor atom with the release of Mn^{2+} from the coordination cavity.[26] Since the replacement of the protonable carboxylate groups with non-protonable amide groups does not allow the formation of the protonated MnHL intermediate, it is likely that the proton assisted dissociation of Mn^{2+} complexes formed with DO2A-bisamides takes place by protonation of the ring N-atom followed by the release of the Mn^{2+} ion. By taking into account the k_1 values of $[Mn(1,4\text{-}BzDO2AM)]^{2+}$, $[Mn(1,4\text{-}DO2AMBz)]^{2+}$ and $[Mn(1,4\text{-}DO2AM)]^{2+}$, it appears that the protonation of the ring N-atom in $[Mn(1,4\text{-}BzDO2AM)]^{2+}$ and $[Mn(1,4\text{-}DO2AMBz)]^{2+}$ occurs more easily, which might be explained by a weaker interaction between the N donor atoms of 1,4-BzDO2AM and 1,4-DO2AMBz ligands and Mn^{2+}. This hypothesis is in line with the lower stability constants of $[Mn(1,4\text{-}BzDO2AM)]^{2+}$ and $[Mn(1,4\text{-}DO2AMBz)]^{2+}$ complexes (Table 1). The half-life ($t_{1/2}$) of dissociation of $[Mn(1,4\text{-}BzDO2AM)]^{2+}$ and $[Mn(1,4\text{-}DO2AMBz)]^{2+}$ calculated for pH = 7.4 is about four times lower than that measured for $[Mn(1,4\text{-}DO2AM)]^{2+}$, but remains significantly longer than those reported for $[Mn(1,4\text{-}DO2A)]$ or $[Mn(1,7\text{-}DO2A)]$.

Table 2. Rate constants and half-lives at pH = 7.4 for the dissociation reactions of $[Mn(1,4\text{-}BzDO2AM)]^{2+}$, $[Mn(1,4\text{-}DO2AMBz)]^{2+}$ and related complexes (0.1 M KCl, 25 °C)

	1,4-BzDO2AM	1,4-DO2AMBz	1,4-DO2AM [d]	1,4-DO2A^{2-} [e]	1,7-DO2A^{2-} [e]	DOTA^{4-} [f]
k_0 (s^{-1})	[a]	[a]	[a]	[a]	[a]	1.8×10^{-7}
k_1 (M^{-1} s^{-1})	36 ± 2	38 ± 2	8.7	99	84	0.04
k_2 (M^{-2} s^{-1}) [b]	—	—	—	1.5×10^6	2.5×10^6	1.6×10^3
log K_{MnLH} [c]	—	—	—	4.15	4.48	4.26
k_d (s^{-1}) pH = 7.4	1.4×10^{-6}	1.5×10^{-6}	3.5×10^{-7}	3.9×10^{-6}	3.3×10^{-6}	2.6×10^{-6}
$t_{1/2}$ (h) pH = 7.4	136	126	556	49.4	58.3	1070

[a] The spontaneous dissociation of the complex characterised by k_0 was found to be negligible. [b] k_2 rate constants characterizing the second-order dependence on H^+ concentration. [c] Protonation constant characterising the protonated intermediate formed prior to complex dissociation. [d] Ref. 19. [e] Ref. 18. [f] Ref. 26.
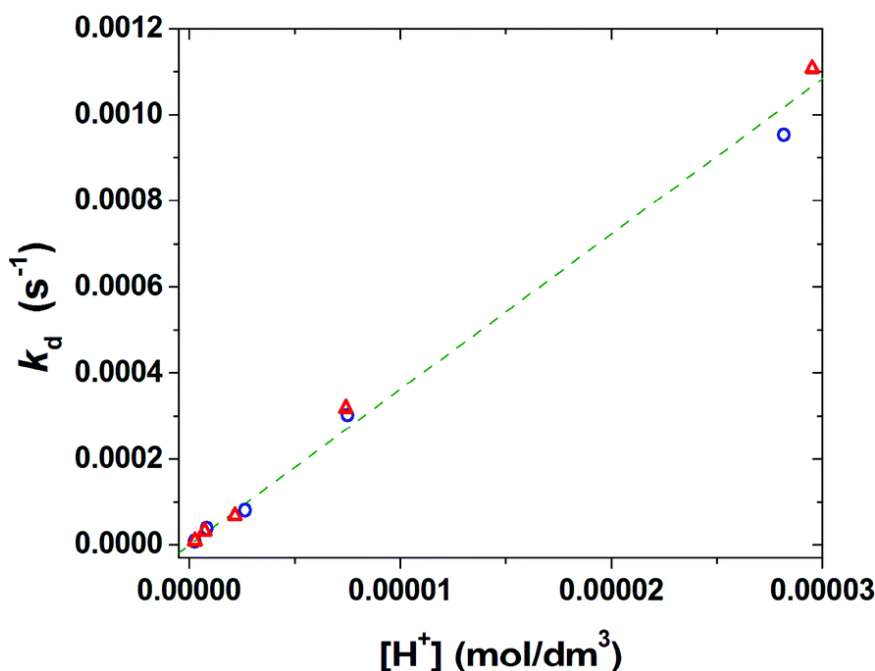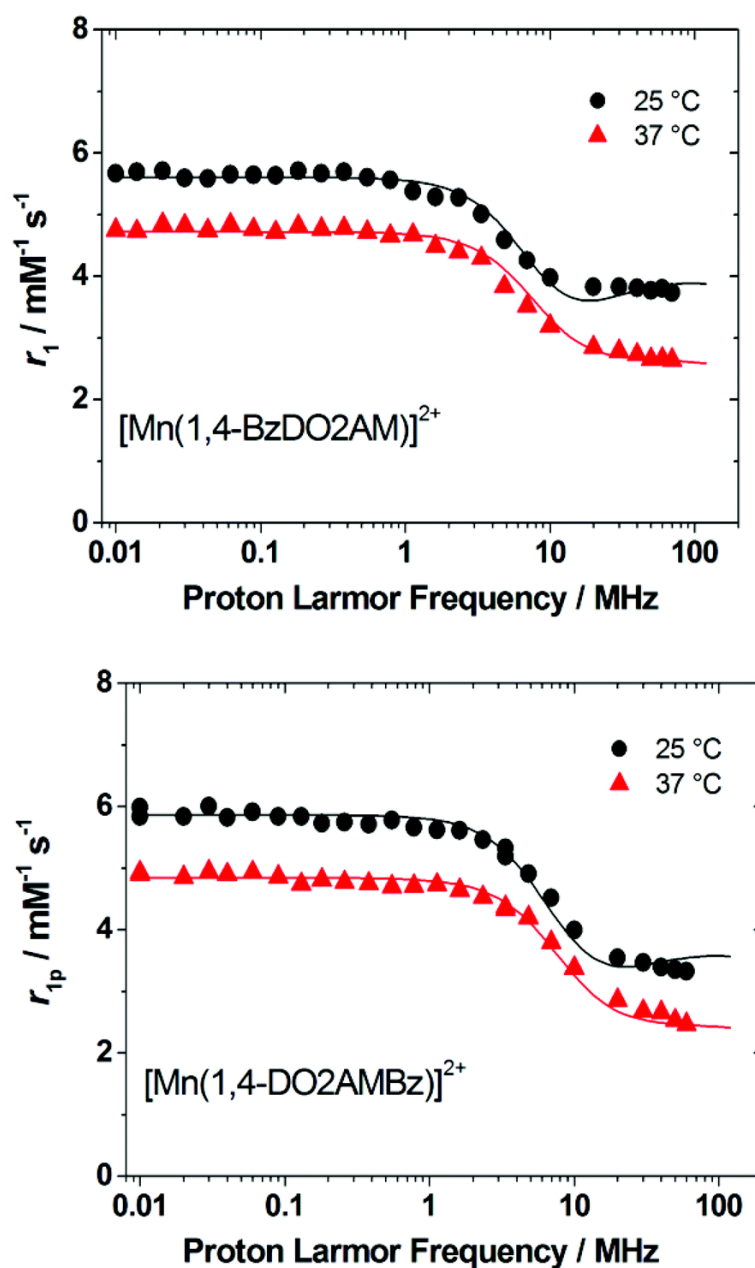
Fig. 2. k_d values obtained for the transmetallation reactions of [Mn(1,4-BzDO2AM)]$^{2+}$ with Zn^{2+} ([MnL] = 0.5 mM, [Zn^{2+}] = 10 mM (blue circles) and 20 mM (red triangles), 0.1 M KCl, 25 °C).

^{1}H and ^{17}O NMR relaxometric studies

The r_{1p} values of [Mn(1,4-BzDO2AM)]$^{2+}$ and [Mn(1,4-DO2AMBz)]$^{2+}$ as measured at 25 °C, 20 MHz and neutral pH are 3.8 and 3.5 mM^{-1} s^{-1}, respectively. These values are considerably higher than that of [Mn(1,4-DO2A)] and [Mn(1,4-DO2AM)]$^{2+}$,[9,19] suggesting that both complexes feature one coordinated water molecule and an enhanced inner sphere relaxivity associated with their larger size (longer τ_R). NMRD profiles were measured at 298 and 310 K over the proton Larmor frequency range 0.01–70 MHz, corresponding to magnetic field strengths varying between 2.343×10^{-4} T and 1.645 T (Fig. 3). The profiles have a rather simple functional form typical of low molecular weight complexes, displaying a region of constant relaxivity at low fields and a simple dispersion around 6–8 MHz, with a second region at high fields (>20 MHz) where the relaxivity tends to flatten out. The absence of a second dispersion at low fields (~1 MHz) indicates that the scalar contribution to relaxivity is negligible.[30]

As for the parent [Mn(1,4-DO2AM)]$^{2+}$ complex, relaxivity decreases by increasing temperature over the entire frequency range, clearly indicating that both Mn^{2+} chelates are in the fast-exchange regime and that r_{1p} is only limited by the rotational correlation time. Given the relatively large number of parameters influencing the relaxivity of Mn^{2+} complexes, the water exchange kinetics of the coordinated water molecules were investigated by analysing the temperature dependence of the ^{17}O NMR transverse relaxation rates (R_2) and paramagnetic chemical shifts ($\Delta\omega$). The experimental data were measured using a high-resolution NMR spectrometer, operating at 11.7 T, on aqueous solutions of the complexes (2–7 mM) at neutral pH. The data were then analysed according to the well-established set of Swift–Connick equations.[31] The reduced R_2 ($1/T_{2r}$) and $\Delta\omega$ values ($\Delta\omega_r$) are presented in Fig. 4. The increase of $1/T_{2r}$ with decreasing temperature over the whole temperature range investigated is a clear indication of a fast rate of exchange for the coordinated water molecule, in agreement with the qualitative analysis of the NMRD profiles recorded at different temperatures.

Fig. 3. ^{1}H NMRD profiles recorded at different temperatures for [Mn(1,4-BzDO2AM)]$^{2+}$ (top) and [Mn(1,4-DO2AMBz)]$^{2+}$ (bottom). The lines represent the fits of the data as explained in the text.

As for the parent [Mn(1,4-DO2AM)]$^{2+}$ complex, relaxivity decreases by increasing temperature over the entire frequency range, clearly indicating that both Mn^{2+} chelates are in the fast-exchange regime and that r_{1p} is only limited by the rotational correlation time. Given the relatively large number of parameters influencing the relaxivity of Mn^{2+} complexes, the water exchange kinetics of the coordinated water molecules were investigated by analysing the temperature dependence of the ^{17}O NMR transverse relaxation rates (R_2) and paramagnetic chemical shifts ($\Delta\omega$). The experimental data were measured using a high-resolution NMR spectrometer, operating at 11.7 T, on aqueous solutions of the complexes (2–7 mM) at neutral pH. The data were then analysed according to the well-established set of Swift–Connick equations.[31] The reduced R_2 ($1/T_{2r}$) and $\Delta\omega$ values ($\Delta\omega_r$) are presented in Fig. 4. The increase of $1/T_{2r}$ with decreasing temperature over the whole temperature range investigated is a clear indication of a fast rate of exchange for the coordinated water molecule, in agreement with the qualitative analysis of the NMRD profiles recorded at different temperatures.

Fig. 4. Reduced transverse ^{17}O NMR relaxation rates and ^{17}O NMR chemical shifts measured for [Mn(1,4-DO2AMBz)]$^{2+}$ (circles) and [Mn(1,4-BzDO2AM)]$^{2+}$ (squares) at 11.74 T. The lines represent the fits of the data as explained in the text.

The ^{1}H NMRD and ^{17}O NMR data were fitted simultaneously according to the established theory of paramagnetic relaxation expressed by the Solomon–Bloembergen–Morgan[32] and Freed[33] equations for the inner- (IS) and outer-sphere (OS) proton relaxation mechanisms, respectively, and the Swift–Connick theory for ^{17}O relaxation.[31] Following a well-established practice, some parameters were fixed at reasonable values due to the large number of parameters that must be considered during the fitting: the hydration number q was fixed at 1; the distance between the metal ion and the protons of the bound water molecule, r, was fixed at 2.83 Å; a and D were set at 3.6 Å and 2.3×10^{-5} cm^2 s^{-1} (at 25 °C), respectively; E_V was fixed at 1.0 kJ mol^{-1}. The values of E_R (activation energy for the rotational motion of the complex) and E_D (activation energy of D) were fixed at those found for [Mn(1,4-DO2A)]: 19.1 and 17.3 kJ mol^{-1}, respectively. The relevant best-fit parameters are listed in Table 3 and compared with those of related macrocyclic Mn^{2+} complexes.

The electron relaxation parameters, Δ^2 and τ_V, are very similar for both macrocyclic complexes and similar to the values found for the parent complex. This represents a strong indication of the occurrence of strictly analogous solution structures for the three complexes. The rotational correlation time τ_R assumes values of 96 and 85 ps for [Mn(1,4-BzDO2AM)]$^{2+}$ and [Mn(1,4-DO2AMBz)]$^{2+}$, respectively. This nicely reflects the increased molecular mass of the benzyl substituted derivatives over the parent complex and confirms the limiting role of the rotational dynamics to the relaxivity of the complexes. In addition, the difference in r_{1p} and τ_R values between the two chelates is well accounted for by their slightly different molecular masses.

The rates of water exchange are about two times that of [Mn(1,4-DO2AM)]$^{2+}$ and approximately half that of [Mn(EDTA)]$^{2-}$. Thus, the introduction of hydrophobic substituents affects not only the rotational dynamics but also the water exchange dynamics of the complexes, likely by influencing the relative energy values of their six- and seven-coordinate states. The seven-coordinate complexes investigated here are expected to follow a dissociatively activated water exchange reaction proceeding through a six-coordinated transition

state. Most likely, the presence of the benzyl groups introduces some steric hindrance around the coordinated water molecule, which facilitates its departure in a dissociatively activated mechanism.

Table 3. Parameters obtained from the simultaneous analysis of ^{17}O NMR and ^{1}H NMRD data

	1,4-BzDO2AM	1,4-DO2AMBz	1,4-DO2AM [b]	1,4-DO2A [c]
r_{1p} at 25/37 °C/mM^{-1} s^{-1} [b]	3.8/2.8	3.5/2.8	2.5/2.0	2.1/1.7
$k_{ex}^{298}/10^6$ s^{-1}	253 ± 9	175 ± 5	111	1134
$\Delta H^{\ddagger}$/kJ mol^{-1}	14.4 ± 1.1	24.6 ± 0.8	39.8	29.4
τ_R^{298}/ps	96 ± 2	85 ± 3	53	46
τ_V^{298}/ps	13 ± 1	11 ± 1	5.5	4.4
E_V/kJ mol^{-1}	1.0 [a]	1.0 [a]	1.0 [a]	1.0 [a]
$\Delta^2/10^{19}$ s^{-2}	20 ± 2	20 ± 1	51	48
$A_O/\hbar/10^6$ rad s^{-1}	-31.0 ± 0.4	-33.0 ± 0.3	-39.0	-43
r_{MnH}/Å	2.83 [a]	2.83 [a]	2.83 [a]	2.83 [a]
a_{MnH}/Å	3.6 [a]	3.6 [a]	3.6 [a]	3.6 [a]
q^{298}	1 [a]	1 [a]	0.87 [a]	0.87 [a]

[a] Parameters fixed during the fitting procedure. [b] Data from Ref. 19. [c] Data from Ref. 9.

<u>DFT calculations</u>

DFT calculations were used to gain insight into the structure of the Mn^{2+} complexes of 1,4-BzDO2AM and 1,4-DO2AMBz in solution. Geometry optimizations were performed on the [Mn(1,4-BzDO2AM)(H$_2$O)]$^{2+}$·2H$_2$O and [Mn(1,4-DO2AMBz)(H$_2$O)]$^{2+}$·2H$_2$O systems, which contain two second-sphere water molecules besides the water molecule directly coordinated to the metal ion. The explicit inclusion of two second-sphere water molecules was found to be critical for an accurate calculation of Mn–O$_{water}$ distances and ^{17}O hyperfine coupling constants $A_O/\hbar$.[11,34] Our calculations provided optimized geometries (Fig. 5) with coordination environments very similar to those calculated previously for [Mn(1,4-DO2A)(H$_2$O)],[9] and that observed in the solid state for [Mn(1,4-DO2A)].[17] Benzylation of the nitrogen atoms of the macrocycle provokes a significant lengthening of the Mn–N distances, which are significantly longer in the complex of 1,4-BzDO2AM compared to the 1,4-DO2AMBz derivative. The spin densities calculated at the nuclei of the coordinated water molecules provide $A_O/\hbar$ values of -52.5×10^6 and -47.3×10^6 rad s^{-1} for the complexes of 1,4-BzDO2AM and 1,4-DO2AMBz, respectively. The calculated values are somewhat higher than those determined experimentally from the analysis of the ^{17}O NMR data (Table 3), but still similar to those reported for different Mn^{2+}complexes. This could be related to the difficulties in the experimental determination of $A_O/\hbar$ values from the observed ^{17}O NMR shifts, or perhaps to the fact that our DFT calculations neglected dynamic effects. Alternatively, a certain fraction of $q = 0$ complexes in solution could explain the lower experimental $A_O/\hbar$ data.
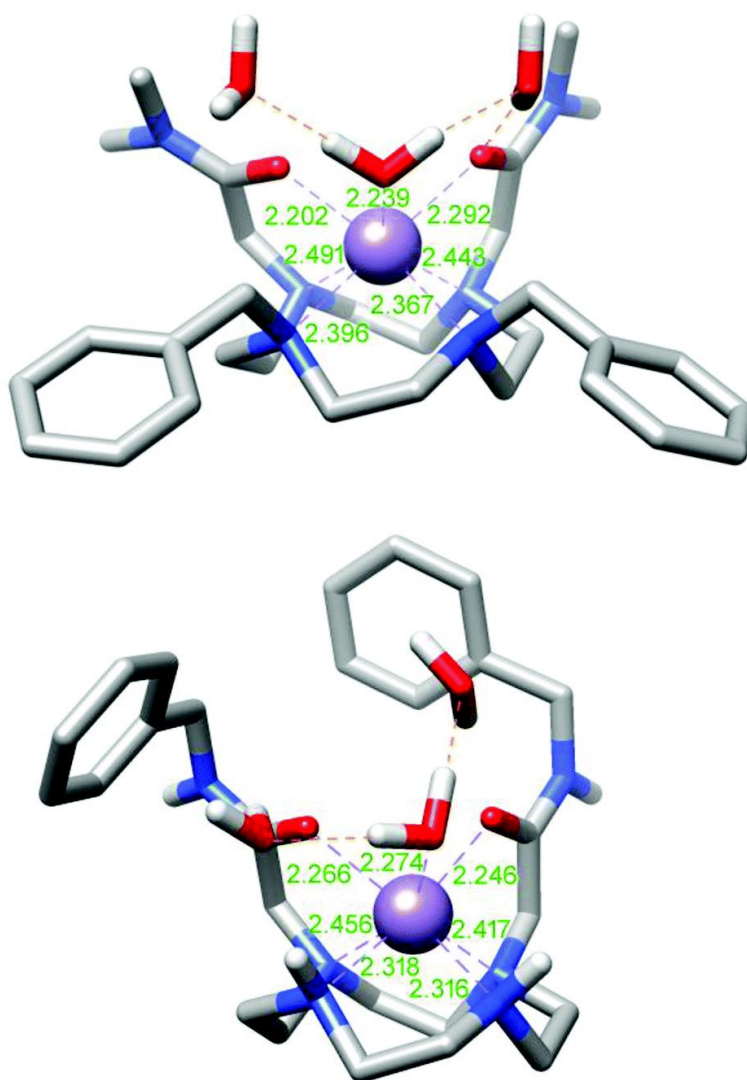
Fig. 5. Structures of the $[Mn(1,4-BzDO2AM)(H_2O)]^{2+} \cdot 2H_2O$ (top) and $[Mn(1,4-DO2AMBz)(H_2O)]^{2+} \cdot 2H_2O$ (bottom) systems obtained with DFT calculations (M062X/TZVP). The bond distances of the metal coordination environments are given in Å.

Human serum albumin (HSA) binding studies

The presence of hydrophobic groups in the structure of 1,4-BzDO2AM and 1,4-DO2AMBz allows the complexes to bind HSA. The binding interaction has been investigated using the well-established proton relaxation enhancement (PRE) technique.[14] This method consists in measuring the increase of the water proton longitudinal relaxation rate (R_1) as a function of increasing concentration of the protein (at 20 MHz and 298 K in the present case, Fig. 6). R_1 is enhanced by the increase of the fraction of the bound complex, characterized by a longer rotational correlation time. The fitting of the experimental data provides the values of the thermodynamic association constant, K_A, the number of equivalent and independent binding sites, n, and the relaxivity of the resulting paramagnetic adduct, r_1^{bound}. All the data were fitted to 1 : 1 binding isotherms even though the presence of multiple affinity sites on HSA cannot be excluded for these complexes. The affinity of the complexes for the protein is influenced by the position of the pendant hydrophobic moieties, with the association constant K_A obtained for $[Mn(1,4-BzDO2AM)]^{2+}$ being *ca.* two times that obtained for $[Mn(1,4-DO2AMBz)]^{2+}$ (Table 4). However, the relaxivity of the fully bound form is

considerably higher for the adduct formed by [Mn(1,4-DO2AMBz)]$^{2+}$, which indicates that the relative position of the benzylic groups in the two complexes influences the motional coupling between the paramagnetic unit and the protein. We hypothesise that the presence of the two hydrophobic groups on the coordinating acetamide moieties limits the degree of local motions involving the coordination cage (longer effective rotational correlation time) and thus increases relaxivity. The association constants obtained for the Mn^{2+} complexes reported here are 2–3 times higher than those reported for Gd^{3+}complexes bearing analogous targeting groups.[35] However, these anionic Gd-chelates differ from the (cationic) Mn^{2+} complexes reported here in their overall charges.
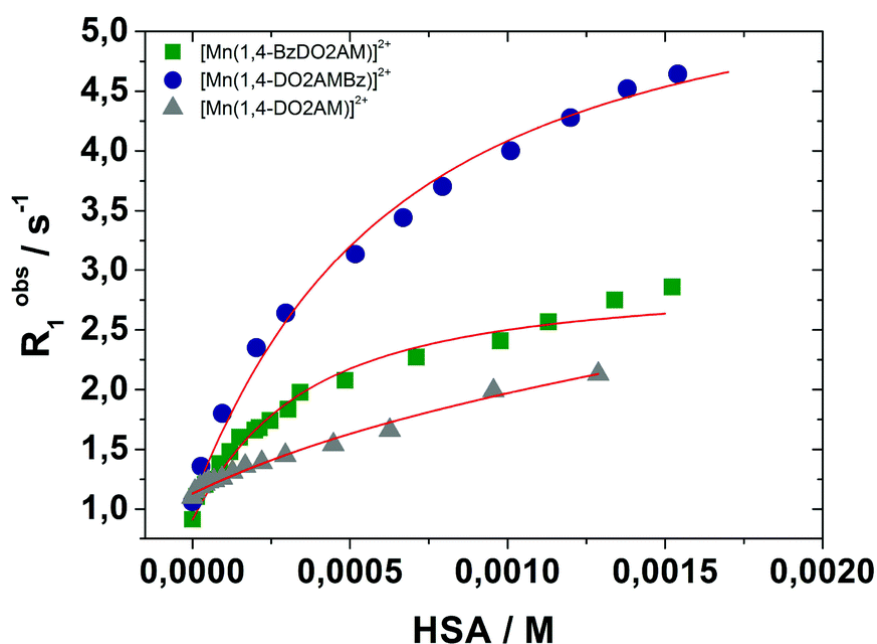
Fig. 6. Changes in the observed longitudinal relaxation rates of water protons observed upon the addition of HSA to solutions of the [Mn(1,4-BzDO2AM)]$^{2+}$ (0.139 mM), [Mn(1,4-DO2AMBz)]$^{2+}$ (0.199 mM) and [Mn(1,4-DO2AM)]$^{2+}$ (0.298 mM) complexes. The solid lines represent the least-squares fits of the data according to a 1 : 1 binding isotherm.

Table 4. Best-fit parameters obtained from the analysis of the ^{1}H relaxometric titrations (20 MHz; 298 K) of the Mn^{2+} complexes of 1,4-BzDO2AM, 1,4-DO2AMBz and 1,4-DO2AM with HAS

	1,4-BzDO2AM	1,4-DO2AMBz	1,4-DO2AM
$n \cdot K_A$ (M^{-1})	3909 ± 583	1964 ± 342	1213 ± 95
$r_{1p}^{\ b}$ (mM^{-1} s^{-1}) ^{a}	18.5 ± 0.7	27.4 ± 1.4	5.6 ± 0.5
$r_{1p}^{\ f}$ (mM^{-1} s^{-1}) ^{b}	3.8	3.5	2.5

^{a} Relaxivity of the complex fully bound to the protein. ^{b} Relaxivity of the free (unbound) complex.

A small but detectable relaxivity enhancement in the presence of HSA is observed also for [Mn(1,4-DO2AM)]$^{2+}$ (Fig. 6). In this case, only electrostatic forces govern the weak interaction and the binding sites

are localized on the negatively charged domain of the protein. The limited relaxivity gain (Table 4) suggests either a marked decrease of the rate of water exchange or a restricted access of bulk solvent molecules to the paramagnetic site. Clearly, the binding sites and the mechanisms of the relaxation enhancement are quite different for the parent $[Mn(1,4-DO2AM)]^{2+}$ complex and the bis-benzyl derivatives. For these latter, the hydrophobic interaction predominates and drives the protein binding event.

Conclusions

The chemical modification of the basic structure of 1,4-DO2AM, with the introduction of two benzyl groups either on the macrocycle or on the pendant arms, has a strong effect on various properties of the corresponding Mn^{2+} complexes. First, the complexes of the benzyl derivatives show higher r_{1p} values. The increase of molecular mass appears to be translated entirely into an increase of relaxivity, thus suggesting a rather compact structure characterised by an isotropic tumbling motion. The high relaxivity values suggest the presence of one bound water molecule, although we cannot exclude the presence of a small population of the $q = 0$ isomer. In any case, the hydration state of the parent complex did not decrease upon the chemical modification. Second, the rate of water exchange has increased by a factor of *ca.* two as compared to the value of $[Mn(1,4-DO2AM)]^{2+}$. This is likely related to the steric compression introduced by the benzyl groups around the water binding site. Third, the presence of the hydrophobic pendant groups enables the formation of non-covalent adducts with HSA, which are characterised by affinity constants and $r_{1p}{}^{b}$ values quite comparable to those typical of the analogous Gd^{3+} complexes.

The results reported in this work also highlight the difficulties to design Mn^{2+} complexes containing a coordinated water molecule and possessing a high thermodynamic stability and kinetic inertness, which represents a challenge for coordination chemistry. The introduction of benzyl groups was found to be detrimental for both the thermodynamic stability and kinetic inertness. These Mn(II) chelates are cationic and thus not suitable for *in vivo* applications. Previous data on lanthanide complexes of DOTA-tetraamide derivatives indicated that at low doses the compounds are not easy to dissociate *in vivo* and are well tolerated.[36] This is due to their high degree of kinetic inertness. In order for the Mn(II) complexes to be employed at high doses *in vivo*, the kinetic inertia and the incorporation of negatively charged groups are important requirements.

We are currently exploring chemical modifications of these and related ligands to obtain efficient and safer Mn^{2+}-based MRI probes.

Experimental section

General

All chemicals were purchased from Sigma-Aldrich Co. and were used without further purification. The concentrations of the $MnCl_2$ and $ZnCl_2$ solutions were determined by complexometric titration with standardised Na_2H_2EDTA and xylenol orange ($ZnCl_2$) or Eriochrome Black T ($MnCl_2$) as indicators. The concentrations of the solutions of 1,4-BzDO2AM and 1,4-DO2AMBz were determined by pH-potentiometric titration in the presence and absence of a 50-fold excess of $CaCl_2$. The pH-potentiometric titrations were carried out with a standardised 0.2 M KOH solution. ^{1}H and ^{13}C NMR spectra were recorded on a Bruker DRX 400 (9.39 T) and a Bruker Avance III (11.74 T) spectrometers. Chemical shifts are reported relative to TMS and were referenced using the residual proton solvent resonances.[37] Electrospray ionization mass spectra (ESI MS) were recorded on an SQD 3100 Mass Detector (Waters), operating in positive or negative ion mode, with 1% v/v HCOOH in methanol as the carrier solvent. HPLC analyses were

carried out on a Waters 1525EF liquid chromatograph equipped with a Waters 2489 UV/vis and a Waters SQD 3100 MS detectors and using a Waters Atlantis® T3 RPC18 column (150 mm × 4.6 mm, 5 μm). Preparative HPLC separations were carried out using a Waters Atlantis® T3 OBD RPC18 column (100 mm × 19 mm, 5 μm) and a Waters FCIII fraction collector.

Synthesis of 2,2′-(1,4,7,10-tetraazacyclododecane-1,4-diyl)bis(*N*-benzylacetamide) (1,4-DO2AMBz)

2-Bromoacetyl bromide (1 mL, 11.5 mmol) and benzyl amine (1.14 mL, 10.4 mmol) were dissolved in CH_2Cl_2 (10 mL) and triethylamine (0.88 mL, 6.26 mmol) was added at 0 °C. The reaction mixture was stirred at 0 °C for 1 h, and then allowed to warm to room temperature. Water (15 mL) was added and the aqueous layer was extracted with CH_2Cl_2 (4 × 15 mL). The combined organic layers were washed with 5% HCl (50 mL), water, a saturated $NaHCO_3$ solution (50 mL) and brine. The organic layer was dried over $MgSO_4$ and then filtered. The solvent was removed under vacuum and the crude product **3** was purified by flash chromatography (petroleum ether : ethyl acetate 7 : 3) on silica gel. The formation of *N*-benzyl-2-bromoacetamide (**3**)[21] was confirmed by mass spectrometry. ESI⁺/MS: *m/z* 228.0 ($[C_9H_{11}BrNO]^+$). Cyclen (0.28 g, 1.6 mmol) was dissolved in acetonitrile (15 mL) and K_2CO_3 (0.33 g, 2.4 mmol) was added. A solution of compound **3** (0.74 g, 3.3 mmol) in the same solvent (20 mL) was added dropwise. The mixture was heated to reflux for 24 h. Then, the solution was filtered to remove the excess of carbonate, and the solvent was removed. The resulting aqueous solution was dried and the crude product was then purified by semi-preparative HPLC-MS (solvent A: H_2O, TFA 0.1%; solvent B: MeOH; 0–2 min 10% B and then gradient 10–100% B in 18 min; flow 20 mL min⁻¹; retention time: 6.3 min) to obtain 140 mg of an orange oil (0.26 mmol, 18% yield). ESI-MS (*m/z*): found 467.5 [M + H⁺] (calc. for $C_{26}H_{38}N_6O_2$: 466.5). ¹H-NMR (D_2O, 500 MHz): δ 3.22 (σ CH_2NH 4H) 3.05 (s, CH_2CO, 4H), 2.85–2.65 (m, NCH_2ring, 16H), 7.51–7.41 (m, CHAr, 10H); ¹³C-NMR (D_2O, 125 MHz): δ 171.4 (C=O), 131.0 (CH), 129.1 (CH), 57.7 (CH_2), 53.5 (CH_2), 53.0 (CH_2), 50.0 (CH_2), 48.9 (CH_2), 36.6 (CH_2).

Synthesis of 2,2′-(7,10-dibenzyl-1,4,7,10-tetraazacyclododecane-1,4-diyl) bis(*N,N*-dimethylacetamide) (1,4-BzDO2AM)

Cyclen (0.5 g, 2.9 mmol) was dissolved in ethanol (15 mL) and diethyl oxalate (585 μL, 4.3 mmol) was added dropwise. The mixture was heated to reflux for 24 h and then the solvent was removed under vacuum to give intermediate 1,4,7,10-tetraazabicyclo[8.2.2]tetradecane-11,12-dione (**4**): ESI⁺/MS: *m/z* 227.2 ($[C_{10}H_{19}N_4O_2]^+$). Compound **4** (0.64 g, 2.8 mmol) was dissolved in acetonitrile (15 mL), and benzyl bromide (840 μL, 7.0 mmol) and K_2CO_3 (2.35 g, 17 mmol) were added to the mixture. The mixture was heated to reflux for 24 h and then the solvent was removed under vacuum. The crude product 4,7-dibenzyl-1,4,7,10-tetraazabicyclo[8.2.2]tetradecane-11,12-dione (**5**) was dissolved in CH_2Cl_2 (20 mL) and washed with water (3 × 15 mL). The product was purified by flash chromatography (98 : 2 DCM : MeOH, silica gel). ESI-MS (*m/z*): found 407.5 [M + H⁺]. Compound **5** was dissolved in 5 M NaOH (20 mL) and the mixture was stirred at 100 °C for 24 h. The solution was concentrated in a rotary evaporator to a volume of 10 mL and washed with CH_2Cl_2 (3 × 20 mL). The combined organic extracts were washed with water (3 × 20 mL). The organic layer was dried over $MgSO_4$ and then filtered and concentrated under vacuum. ESI-MS (*m/z*): found 353.5 [M + H⁺]. The intermediate was used without any further characterization.[23] Compound **6** (0.17 g, 0.5 mmol) and K_2CO_3 (0.63 g, 4.5 mmol) were suspended in ACN (10 ml) and *N,N*-dimethyl-2-chloroacetamide (105 μL, 1.01 mmol) was added dropwise. The mixture was stirred for 24 h and then the solvent was removed *in vacuo*. The crude product **8** was purified by flash chromatography (DCM : MeOH 99 : 1, silica gel) to obtain a pale yellow oil (0.46 mmol, 16% yield). ESI-MS (*m/z*): found 523.5 [M + H⁺] (calc. for $C_{30}H_{46}N_6O_2$: 522.5). ¹H-NMR (D_2O, 500 MHz): δ 4.31 (σ CH_2 4H) 3.18 (s, CH_2CO, 4H), 3.51 (s CH_3 12H) 2.01–2.28 (m, NCH_2 ring, 16H), 7.30–7.37 (m, CHAr, 10H); ¹³C-NMR (D_2O, 125 MHz): δ 172.5 (C=O), 137.8 (CH), 126.5.0 (CH), 127.0 (CH), 127.6 (CH) 49.5 (CH_2), 50.1 (CH_2), 50.6 (CH_2), 51.2 (CH_2), 51.9 (CH_2), 55.0 (CH_2) 41.9 (CH_3).

Equilibrium measurements

The protonation constants of 1,4-BzDO2AM and 1,4-DO2AMBz, as well as the stability and protonation constants of the Mn^{2+}complexes formed with 1,4-BzDO2AM and 1,4-DO2AMBz were determined by pH-potentiometry. The pH-potentiometic titrations were performed at 1 : 1 metal-to-ligand concentration ratios (the concentration of the ligand was generally 0.002 M). For the calculation of the equilibrium constants the mL base–pH data were used, obtained in the pH range 1.7–12.0. For the pH measurements and titrations, a Metrohm 888 Titrando titration workstation and a Metrohm 6.0233.100 combined electrode were used. Equilibrium measurements were carried out at a constant ionic strength (0.1 M KCl) and at 25 °C in 8 mL samples. The solutions were stirred, and N_2 was bubbled through them. KH-phthalate (pH = 4.005) and borax (pH = 9.177) buffers were used to calibrate the pH meter. For the calculation of $[H^+]$ from the measured pH values, the method proposed by Irving et al.was used.[38] A 0.01 M HCl solution was titrated with the standardized KOH solution in the presence of 0.1 M KCl ionic strength, respectively. The differences between the measured (pH_{read}) and calculated pH ($-log[H^+]$) values were used to obtain the equilibrium H^+ concentration from the pH values, measured in the titration experiments. The ion product of water was determined from the same titrations (HCl/KOH) using the data in the pH range of 11.5–12.0. Equilibrium constants were calculated using the PSEQUAD program.[39]

Kinetic studies

The kinetic inertness of the Mn^{2+} complexes was characterised by the rates of the exchange reactions taking place between the MnL complexes and Zn^{2+}. The rates of the metal exchange reactions of $[Mn(1,4-BzDO2AM)]^{2+}$ and $[Mn(1,4-DO2AMBz)]^{2+}$ with Zn^{2+} were followed by measuring the water proton relaxation rates ($1/T_1$) of the samples. The kinetic measurements were performed at 0.47 T (20 MHz) and 25 °C owing to the large differences in the relaxivities of $[Mn(1,4-BzDO2AM)]^{2+}$ (r_{1p} = 3.8 $mM^{-1}s^{-1}$) and $[Mn(1,4-DO2AMBz)]^{2+}$ (r_{1p} = 3.5 $mM^{-1} s^{-1}$) and that of free Mn^{2+} (r_{1p} = 8.0 $mM^{-1} s^{-1}$). The longitudinal relaxation times were measured by the inversion recovery method ($180° - \tau - 90°$) by using 8 different τ values. The measurements were performed with 1.0 mM $[Mn(1,4-BzDO2AM)]^{2+}$ and $[Mn(1,4-DO2AMBz)]^{2+}$ solutions in the presence of a 10 to 20-fold excess of Zn^{2+}. The temperature was maintained at 25 °C and the ionic strength of the solutions was kept a constant (0.1 M KCl). For keeping the pH values constant, N-methylpiperazine (pH range of 4.1–5.2) and piperazine (pH range of 4.7–6.6) buffers (0.01 M) were used. The pseudo-first-order rate constants (k_d) were calculated using eqn (9):

$$R_1^t = (R_1^0 - R_1^e)e^{-k_d t} + R_1^e \qquad (9)$$

where R^0_1, R^t_1, and R^e_1 are the relaxation rate ($1/T_1$) values at the start of the reaction, at time t, and at equilibrium, respectively. The calculations were performed using the computer program Micromath Scientist, version 2.0 (Salt Lake City, UT, USA).

^{1}H NMRD and ^{17}O NMR measurements

The water proton longitudinal relaxation rates as a function of pH (20 MHz) were measured with a Stelar Spinmaster Spectrometer FFC-2000 (Mede, PV, Italy) on about 0.6–2.0 mM aqueous solutions in non-deuterated water. The exact concentrations of Mn^{2+} ions were determined by the measurement of bulk magnetic susceptibility shifts of a ^{t}BuOH signal on a Bruker Avance III spectrometer (11.7 T).[40] The ^{1}H T_1 relaxation times were acquired by the standard inversion recovery method with a typical 90° pulse width of 3.5 μs, 16 experiments of 4 scans each. The reproducibility of the T_1 data was ±5%. The temperature was controlled with a Stelar VTC-91 airflow heater equipped with a calibrated copper-

constantan thermocouple (uncertainty of ±0.1 °C). The proton $1/T_1$ NMRD profiles were measured on a fast field-cycling Stelar SmartTracer relaxometer over a continuum of magnetic field strengths from 0.00024–0.25 T (corresponding to 0.01–10 MHz proton Larmor frequencies). The relaxometer operates under computer control with an absolute uncertainty in $1/T_1$ of ±1%. Additional data points in the range 15–70 MHz were obtained on a Stelar relaxometer equipped with a Bruker WP80 NMR electromagnet adapted to variable-field measurements (see above).

Variable-temperature ^{17}O NMR measurements were recorded on a Bruker Avance III spectrometer (11.7 T) equipped with a 5 mm probe and a standard temperature control unit. Aqueous solutions of the complexes (4 mM) containing 2.0% of the ^{17}O isotope (Cambridge Isotope) were used. The observed transverse relaxation rates were calculated from the signal width at half-height.

DFT calculations

Full geometry optimizations of the $[Mn(1,4\text{-}DO2AMBz)(H_2O)]^{2+} \cdot 2H_2O$ and $[Mn(1,4\text{-}BzDO2AM)(H_2O)]^{2+} \cdot 2H_2O$ systems were performed employing DFT calculations at the M062X/TZVP[41,42] level with the Gaussian 09 package (revision D.01).[43] Solvent effects were included by using the polarizable continuum model (PCM), in particular, the integral equation formalism (IEFPCM) variant.[44] No symmetry constraints have been imposed during the optimizations. The stationary points found on the potential energy surfaces as a result of geometry optimizations were characterized *via* frequency analysis. Hyperfine coupling constants were calculated with the same computational approach using the EPR-III basis set of Barone for C, H, O and N.[45]

References

1. (*a*) G. J. Stasiuk and N. J. Long, *Chem. Commun.*, 2013, **49**, 2732; (*b*) P. Caravan, J. J. Ellison, T. J. McMurry and R. B. Lauffer, *Chem. Rev.*, 1999, **99**, 2293; (*c*) N. Cakić, S. Gündüz, R. Rengarasu and G. Angelovski, *Tetrahedron Lett.*, 2015, **56**, 759; (*d*) R. E. Mewis and S. J. Archibald, *Coord. Chem. Rev.*, 2010, **254**, 1686; (*e*) M. C. Heffern, L. M. Matosziuk and T. J. Meade, *Chem. Rev.*, 2014, **114**, 4496.

2. *The Chemistry of Contrast Agents in Medical Magnetic Resonance Imaging*, ed. A. E. Merbach, L. Helm and É. Tóth, 2nd edn, Wiley, New York, 2013.

3. (*a*) P. Blower, *Dalton Trans.*, 2006, 1705; (*b*) K. Tanaka and K. Fukase, *Org. Biomol. Chem.*, 2008, **6**, 815.

4. (*a*) E. Vinogradova, A. D. Sherry and R. E. Lenkinski, *J. Magn. Reson.*, 2013, **229**, 155; (*b*) E. Terreno, D. Delli Castelli and S. Aime, *Contrast Media Mol. Imaging*, 2010, **5**, 78; (*c*) G. Ferrauto, D. Delli Castelli, E. Di Gregorio, E. Terreno and S. Aime, *Wiley Interdisc. Rev.: Nanomed. Nanobiotechnol.*, 2016, **8**, 602.

5. J.-C. G. Bünzli, *Chem. Rev.*, 2010, **110**, 2729.

6. E. Brücher, G. Tircsó, Z. Baranyai, Z. Kovács and A. D. Sherry, Stability and Toxicity of Contrast Agents, in *The Chemistry of Contrast Agents in Medical Magnetic Resonance Imaging*, ed. A. E. Merbach, L. Helm and É. Tóth, 2nd edn, Wiley, New York, 2013, ch. 4, pp. 157–208.

7. (*a*) D. Pan, A. H. Schmieder, S. A. Wickline and G. M. Lanza, *Tetrahedron*, 2011, **67**, 8431; (*b*) B. Drahos, I. Lukes and E. Toth, *Eur. J. Inorg. Chem.*, 2012, 1975; (*c*) M. Kueny-Stotz, A. Garofalo and D. Felder-Flesch,*Eur. J. Inorg. Chem.*, 2012, 1987.

8. (*a*) J. Zhu, E. M. Gale, I. Atanasova, T. A. Rietz and P. Caravan, *Chem. – Eur. J.*, 2014, **20**, 14507; (*b*) E. M. Gale, I. P. Atanasova, F. Blasi, I. Ay and P. Caravan, *J. Am. Chem. Soc.*, 2015, **137**, 15548.

9. G. A. Rolla, C. Platas-Iglesias, M. Botta, L. Tei and L. Helm, *Inorg. Chem.*, 2013, **52**, 3268.

10. L. Tei, G. Gugliotta, M. Fekete, F. K. Kalman and M. Botta, *Dalton Trans.*, 2011, **40**, 2025.

11. (*a*) E. Molnar, N. Camus, V. Patinec, G. A. Rolla, M. Botta, G. Tircso, F. K. Kalman, T. Fodor, R. Tripier and C. Platas-Iglesias,*Inorg. Chem.*, 2014, **53**, 5136; (*b*) V. Patinec, G. A. Rolla, M. Botta, R. Tripier, D. Esteban-Gómez and C. Platas-Iglesias, *Inorg. Chem.*, 2013, **52**, 11173.

12. (*a*) M. Regueiro-Figueroa, G. A. Rolla, D. Esteban-Gómez, A. de Blas, T. Rodríguez-Blas, M. Botta and C. Platas-Iglesias,*Chem. – Eur. J.*, 2014, **20**, 17300; (*b*) A. Forgacs, M. Regueiro-Figueroa, J. L. Barriada, D. Esteban-Gómez, A. de Blas, T. Rodríguez-Blas, M. Botta and C. Platas-Iglesias, *Inorg. Chem.*, 2015, **54**, 9576.

13. A. Forgacs, R. Pujales-Paradela, M. Regueiro-Figueroa, L. Valencia, D. Esteban-Gómez, M. Botta and C. Platas-Iglesias,*Dalton Trans.*, 2017, **46**, 1546.

14. A. de Sa, C. S. Bonnet, C. F. G. C. Geraldes, É. Tóth, P. M. T. Ferreira and J. P. Andre, *Dalton Trans.*, 2013, **42**, 4522.

15. (*a*) S. Aime, P. L. Anelli, M. Botta, M. Brocchetta, S. Canton, F. Fedeli, E. Gianolio and E. Terreno, *J. Biol. Inorg. Chem.*, 2002,**7**, 58; (*b*) R. Artali, Z. Baranyai, M. Botta, G. B. Giovenzana, A. Maspero, R. Negri, G. Palmisano, M. Sisti and S. Tollari, *New J. Chem.*, 2015, **39**, 539.

16. (*a*) G. S. Loving, S. Mukherjee and P. Caravan, *J. Am. Chem. Soc.*, 2013, **135**, 4620; (*b*) E. M. Gale, S. Mukherjee, C. Liu, G. S. Loving and P. Caravan, *Inorg. Chem.*, 2014, **53**, 10748.

17. A. Bianchi, L. Calabi, C. Giorgi, P. Losi, P. Mariani, D. Palano, P. Paoli, P. Rossi and B. Valtancoli, *J. Chem. Soc., Dalton Trans.*, 2001, 917.

18. Z. Garda, A. Forgacs, Q. N. Do, F. K. Kalman, S. Timari, Z. Baranyai, L. Tei, I. Toth, Z. Kovacs and G. Tircso, *J. Inorg. Biochem.*, 2016, **163**, 206.

19. A. Forgacs, L. Tei, Z. Baranyai, I. Toth, L. Zekany and M. Botta, *Eur. J. Inorg. Chem.*, 2016, 1165.

20. S. Aime, M. Botta, M. Fasano, S. Geninatti Crich and E. Terreno, *J. Biol. Inorg. Chem.*, 1996, **1**, 312.

21. H. Xie, D. Ng, S. N. Savinov, B. Dey, P. D. Kwong, R. Wyatt, A. B. Smith and W. A. Hendrickson, *J. Med. Chem.*, 2007, 4898.

22. (*a*) C. Li and W.-T. Wong, *J. Org. Chem.*, 2003, **68**, 2956; (*b*) W. J. Kruper Jr., P. R. Rudolf and C. A. Langhoff, *J. Org. Chem.*, 1993, **58**, 3869.

23. F. Bellouard, F. Chuburu, N. Kervarec, L. Toupet, S. Triki, Y. Le Mest and H. Handel, *J. Chem. Soc., Perkin Trans. 1*, 1999, 3499.

24. A. Z. Garda, E. Ruscsak, D. Esteban-Gomez, A. de Blas, T. Rodriguez-Blas, L. N. P. Lima, M. Beyler, R. Tripier, G. Tircso and C. Platas-Iglesias, *Dalton Trans.*, 2015, **44**, 5017.

25. (*a*) A. Pasha, G. Tircsó, E. T. Benyo, E. Brucher and A. D. Sherry, *Eur. J. Inorg. Chem.*, 2007, 4340; (*b*) Zs. Baranyai, E. Brücher, T. Iványi, R. Király, I. Lázár and L. Zékány, *Helv. Chim. Acta*, 2005, **88**, 604–617.

26. B. Drahos, V. Kubicek, C. S. Bonnet, P. Hermann, I. Lukes and É. Tóth, *Dalton Trans.*, 2011, **40**, 1945.

27. R. D. Shannon, *Acta Crystallogr., Sect. A: Cryst. Phys., Diffr., Theor. Gen. Cryst.*, 1976, **32**, 751.

28. J. Crossgrove and W. Zheng, *NMR Biomed.*, 2004, **17**, 544.

29. P. Wedeking, K. Kumar and M. F. Tweedle, *Magn. Reson. Imaging*, 1992, **10**, 641.

30. D. Esteban-Gómez, C. Cassino, M. Botta and C. Platas-Iglesias, *RSC Adv.*, 2014, **4**, 7094.

31. (*a*) T. J. Swift and R. E. Connick, *J. Chem. Phys.*, 1962, **37**, 307; (*b*) T. J. Swift and R. E. Connick, *J. Chem. Phys.*, 1964, **41**, 2553.

32. (*a*) I. Solomon, *Phys. Rev.*, 1955, **99**, 559; (*b*) I. Solomon and N. Bloembergen, *J. Chem. Phys.*, 1956, **25**, 261; (*c*) N. Bloembergen, *J. Chem. Phys.*, 1957, **27**, 572; (*d*) N. Bloembergen and L. O. Morgan, *J. Chem. Phys.*, 1961, **34**, 842.

33. J. H. Freed, *J. Chem. Phys.*, 1978, **68**, 4034.

34. C. Platas-Iglesias, D. Esteban-Gómez, L. Helm and M. Regueiro-Figueroa, *J. Phys. Chem. A*, 2016, **120**, 6467–6476.

35. S. Aime, M. Botta, M. Fasano, S. Geninatti Crich and E. Terreno, *J. Biol. Inorg. Chem.*, 1996, **1**, 312.

36. M. Woods, P. Caravan, C. F. G. C. Geraldes, M. T. Greenfield, G. E. Kiefer, M. Lin, K. McMillan, M. I. M. Prata, A. C. Santos, X. Sun, J. Wang, S. Zhang, P. Zhao and A. D. Sherry, *Invest. Radiol.*, 2008, **43**, 861.

37. H. E. Gottlieb, K. Kottyar and A. Nudelman, *J. Org. Chem.*, 1997, **62**, 7512.

38. H. M. Irving, M. G. Miles and L. Pettit, *Anal. Chim. Acta*, 1967, **38**, 475.

39. L. Zékány and I. Nagypál, in *Computational Method for Determination of Formation Constants*, ed. D. J. Legett, Plenum, New York, 1985, p. 291.

40. D. M. Corsi, C. Platas-Iglesias, H. van Bekkum and J. A. Peters, *Magn. Reson. Chem.*, 2001, **39**, 723.

41. Y. Zhao and D. G. Truhlar, *Theor. Chem. Acc.*, 2008, **120**, 215.

42. A. Schaefer, C. Huber and R. Ahlrichs, *J. Chem. Phys.*, 1994, **100**, 5829.

43. M. J. Frisch, *et al.* Gaussian, Inc., Wallingford, CT, 2009.

44. J. Tomasi, B. Mennucci and R. Cammi, *Chem. Rev.*, 2005, **105**, 2999.

45. N. Rega, M. Cossi and V. Barone, *J. Chem. Phys.*, 1996, **105**, 11060.